THE JOURNAL OF PHYSICAL CHEMISTRY C

Article

pubs.acs.org/JPCC

Effects of Precursor Ratios and Annealing on Electronic Structure and Surface Composition of $CH_3NH_3PbI_3$ Perovskite Films

Haipeng Xie,[†] Xiaoliang Liu,*[,†] Lu Lyu,[†] Dongmei Niu,[†] Qi Wang,[‡] Jinsong Huang,[‡] and Yongli Gao*[,§]

[†]Institute of Super-Microstructure and Ultrafast Process in Advanced Materials, School of Physics and Electronics, Central South University, Changsha, Hunan 410083, China

[‡]Department of Mechanical and Materials Engineering and Nebraska Center for Materials and Nanoscience, University of Nebraska-Lincoln, Lincoln, Nebraska 68588-0656, United States

[§]Department of Physics and Astronomy, University of Rochester, Rochester, New York 14627, United States

Supporting Information

ABSTRACT: The electronic structure and surface composition of $CH_3NH_3PbI_3$ ($MAPbI_3$) films fabricated by one-step method with different precursor ratios of PbI_2 to CH_3NH_3I (PbI_2/MAI) have been investigated with ultraviolet photoelectron spectroscopy (UPS) and X-ray photoelectron spectroscopy (XPS). It is found that the core levels of all components in the $MAPbI_3$ film shift toward lower binding energy with decreasing the precursor ratio of PbI_2/MAI, indicating that the electronic structures of the $MAPbI_3$ film can be adjusted by the precursor ratio of PbI_2/MAI. The elemental compositions of the $MAPbI_3$ film also depend on the precursor ratio and annealing process, and the compositions are strongly correlated to the electronic properties of the films. The electronic properties remain unchanged with an annealing at 110 °C. However, a core level shift of 0.5 eV toward higher binding energy is observed with an annealing at 150 °C, together with noticeable composition change from the XPS core level analysis. The distribution of all chemical components in the $MAPbI_3$ film is further investigated with angle-resolved XPS (AR-XPS). It is observed that annealing at 150 °C leads to relatively shallow distribution variations of I and Pb in the $MAPbI_3$ film, accompanied by infiltration of metallic Pb into the bulk.

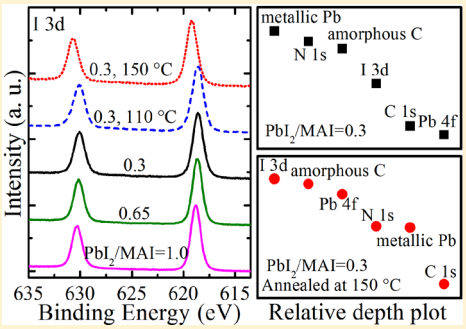

1. INTRODUCTION

Organometallic halide perovskites have attracted intensive interests in recent years due to their excellent characteristics of high absorption coefficient, appropriate direct bandgap, nice carrier transport, low cost, and solution-based fabrication process.[1−4] There have been unexpected breakthroughs and rapid evolution of highly efficient solar cells based on this kind of perovskite materials in the past few years. A 3.8% efficient dye-sensitized solar cell (DSSC) based on perovskite $CH_3NH_3PbI_3$ ($MAPbI_3$) was first reported by Kojima et al. in 2009.[5] After a short time, Snaith's group demonstrated that a planar heterojunction $MAPbI_3$ solar cell without the mesoporous electrode in typical sensitized solar cells could have very high efficiency of 12.3%.[6] Then, Grätzel et al. brought the efficiency to 15.0% by depositing $MAPbI_3$ on nanoporous TiO_2.[7] Bi et al. achieved a stabilized efficiency of near 19.0% by applying nonwetting high-aspect-ration crystalline grain growth for $MAPbI_3$ solar cells.[8] Recently, a power conversion efficiency of 20.1% was certified by the National Renewable Energy Laboratory.[9] It is expected that the stabilized efficiency of 20% or higher can be reached by optimizing the device structures and interface modifications.

To date, $MAPbI_3$ films have been formed by versatile film deposition approaches such as single-step premixed precursor deposition by spin-coating, sequential deposition of precursors, and coevaporation of the precursors.[10−14] Among all the possible methods, the solution process has proven to be an appropriate method to create high quality $MAPbI_3$ film due to its low cost, large scale, and flexible environmental conditions. Recent development of solution chemistry engineering has been confirmed to lead to fabrication of high efficiency solar cells.[15] Seok et al. reported an efficiency of 16.5% in solution-processed $MAPbI_3$ solar cells by the preparation of extremely uniform $MAPbI_3$ layers.[16] Lee et al. reported that the power conversion efficiency of solution-processed $MAPbI_3$-based devices could be improved by surface modification.[17,18] Wang et al. reported recently that the surface morphology and devices performance were significantly modified by controlling the precursor ratio of PbI_2 to CH_3NH_3I (MAI).[19,20] Substantial achievements in the solution fabrication techniques of $MAPbI_3$ film have been reported so far. However, some basic problems in solution process still remain unsolved, such as the precise relation between the surface composition of $MAPbI_3$ films and the precursor ratios of PbI_2 to MAI (PbI_2/MAI) in mixed solution and the distribution of chemical components in $MAPbI_3$ films for the as-grown and annealed $MAPbI_3$ films. We

Received: August 8, 2015
Revised: December 13, 2015
Published: December 14, 2015

DOI: 10.1021/acs.jpcc.5b07728
J. Phys. Chem. C 2016, 120, 215−220

have observed that changing the precursor ratios can control the electrical doping properties of $MAPbI_3$ films.[19] However, the underlying mechanisms for the control of the electronic properties still remain to be investigated.

In this paper, we report our systematic investigations on the electronic structure, surface composition, and the component distribution of the $MAPbI_3$ films fabricated by one-step method with different precursor ratios using ultraviolet photoelectron spectroscopy (UPS), X-ray and angle-resolved X-ray photoelectron spectroscopy (XPS, AR-XPS). The core level shifts of the $MAPbI_3$ films observed by XPS show that its electronic structures are strongly correlated to the precursor ratio. The electronic structure of $MAPbI_3$ film can also be changed by implementing an appropriate annealing process. The AR-XPS shows that there is more I and Pb in the surface region than in the bulk, and the metallic Pb infiltrates into the bulk for the $MAPbI_3$ film annealed at 150 °C. The analysis therefore provides a comprehensive picture of the microscopic dependence of the electronic structure on compositions in hybrid perovskite.

2. EXPERIMENTAL SECTION

$MAPbI_3$ film was prepared by using single-step premixed precursor deposition as recently reported.[19] First, poly(3,4-ethylenedioxythiophene)/poly(styrenesulfonate) (PEDOT:PSS) was spun coated onto the ITO substrate at 3000 rounds per minute (rpm) for 60 s, and then followed by 105 °C annealing for 30 min. The different PbI_2/MAI ratios of 0.3, 0.65, and 1.0 were obtained by mixing in different proportions of PbI_2 and MAI that were dissolved in anhydrous *N*,*N*-dimethylformamide (DMF) at the concentration of 400 mg/mL. The mixture solutions were spun coated onto ITO/PEDOT:PSS at a rate of 9000 rpm for 30 s. Then the $MAPbI_3$ films were annealed at 100 °C for 60 min. The thickness of $MAPbI_3$ films is ca. 250 nm.

The three kinds of as-grown $MAPbI_3$ films were sent into the characterization chamber for UPS and XPS measurements. The UPS was measured with a SPECS Microwave UV Light Source (He I = 21.2 eV) and XPS with monochromatic SPECS XR-MF Microwave X-ray source (Al K_α = 1486.7 eV) in an ultrahigh vacuum (UHV) system.[21−24] The UHV system includes a SPECS PHOIBOS 150 hemispherical energy analyzer and the based pressure is superior to 2×10^{-10} mbar. A total energy resolution of 70 meV was selected for the UPS measurements as determined from the Fermi edge of Au. For XPS, the resolution of the spectrometer was chosen to be 0.65 eV with the pass energy setting of 40 eV. After the UPS and XPS measurements, a 110 °C annealing for 30 min was carried out for each $MAPbI_3$ film, then the samples were sent back to the characterization chamber to collect their UPS and XPS data. For the $MAPbI_3$ film fabricated with the precursor ratio of 0.3, an additional annealing at 150 °C for 45 min was applied in order to verify the annealing effect on the electronic structure of the $MAPbI_3$ film. The binding energies of all UPS and XPS spectra were calibrated and referenced to the Fermi level (E_F) of the sample. Atomic force microscopy (AFM) imaging was examined by Agilent 5500AFM/SPM using the tapping mode. All measurements were taken at room temperature.

3. RESULTS AND DISCUSSION

Shown in Figure 1a are the XPS full scan spectra of $MAPbI_3$ films coated on the top of an ITO/PEDOT:PSS substrate with

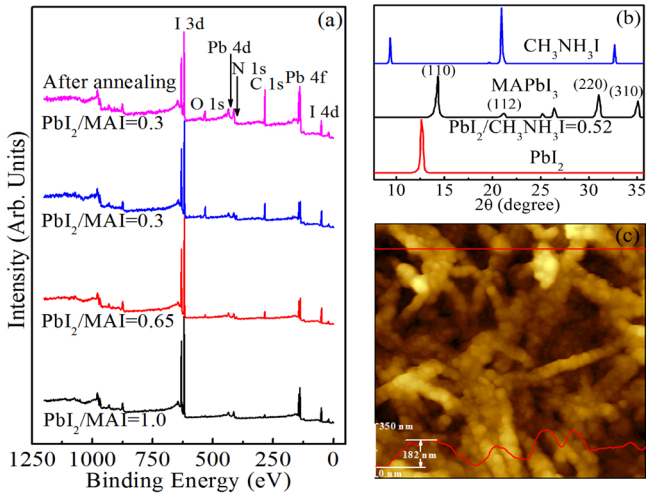

Figure 1. (a) The XPS full scan spectra of the $MAPbI_3$ films coated on the top of an ITO/PEDOT:PSS substrate with precursor ratios of 1.0, 0.65, 0.3, and 0.3 annealed at 150 °C for 45 min. (b) The XRD spectra of $MAPbI_3$ film prepared with the precursor ratio of 0.52 accompanied by those of MAI and PbI_2. (c) The AFM image (5 μm × 5 μm) of the $MAPbI_3$ film with 1.0 precursor ratio. The cross-sectional profiles corresponding to the line is shown at the bottom.

precursor ratios PbI_2/MAI of 1.0, 0.65, 0.3, and 0.3 followed by annealing at 150 °C for 45 min. To eliminate the surface charging effects, we use the amorphous carbon C 1s core level of 284.5 eV as a reference to calibrate the energy position of all the spectra. As expected, the sample displays carbon, nitrogen, iodine, lead, and oxygen. It is worth to note that no sulfur component was detected in the XPS spectra of $MAPbI_3$ film for all samples despite being a basic component of the underneath PEDOT:PSS substrate, indicating that the XPS signal from the PEDOT:PSS substrate can be completely suppressed by such a thickness of 250 nm $MAPbI_3$ overlayer in spite of its possibly poor surface coverage. Therefore, the slight presence of oxygen might be ascribed to the contamination from the ex situ XPS characterization rather than the oxygen component of PEDOT:PSS. The XPS full scan spectra just provide simple information about the $MAPbI_3$ films. We find it difficult to identify significant difference among the four full scan spectra.

Figure 1b presents the XRD patterns of $MAPbI_3$ film prepared with the precursor ratio of 0.52 accompanied by those of PbI_2 and MAI. It is observed that the impurity peaks of PbI_2 and MAI almost completely disappear as the precursor ratio increases from 0.3 to ca. 0.52 and the XRD patterns remain almost unchanged with the subsequent increase of the precursor ratio. The results observed here are in good agreement with the previous report.[21] The nonunit precursor ratio for stoichiometric $MAPbI_3$ film formation indicates that the composition of the spun films is different from that in the precursor solution, which should be ascribed to the different affinities of MAI and PbI_2 to the substrates. Shown in Figure 1c is the AFM image of $MAPbI_3$ film with precursor ratio of 1.0. A $MAPbI_3$ film with high roughness (ca. 65 nm) and a lot of microfibers is observed, likely due to the high content of PbI_2. The cross-sectional profiles corresponding to the line is shown

DOI: 10.1021/acs.jpcc.5b07728
J. Phys. Chem. C 2016, 120, 215−220

at the bottom. It is found that the maximum difference of ca.182 nm in height is less than the thickness of $MAPbI_3$ films.

Presented in Figure 2 are the XPS spectra of C 1s, N 1s, I $3d_{5/2}$, and Pb $4f_{7/2}$ of $MAPbI_3$ films fabricated with different

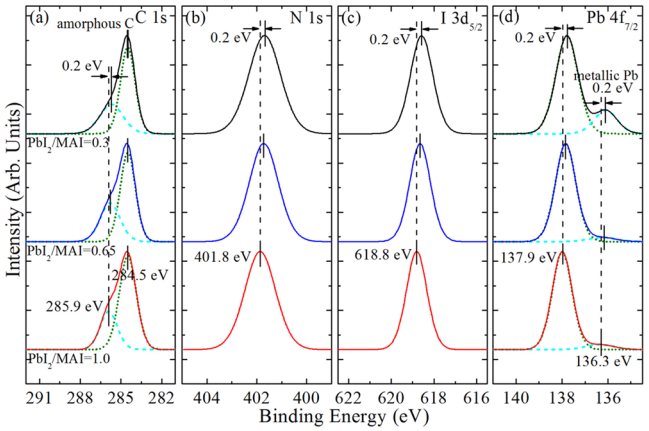

Figure 2. XPS spectra of (a) C 1s, (b) N 1s, (c) I $3d_{5/2}$, and (d) Pb $4f_{7/2}$ for $MAPbI_3$ films fabricated with different precursor ratios of 1.0, 0.65, and 0.3 from the bottom to the top.

precursor ratios. The spectra have been normalized to the same height for visual clarity. The areas of the XPS spectra of the elements were obtained by fitting Lorentzian−Gaussian peaks after removing the secondary electron background, followed by normalization with corresponding atomic sensitivity factors. We find that the binding energies (BE) of C 1s, N 1s, I $3d_{5/2}$, and Pb $4f_{7/2}$ core level slightly shift (~0.2 eV) to low BE as the precursor ratio decreases from 1.0 to 0.3, almost following the same trend of the valence band maximum (VBM) shift observed by the UPS results in our previous works.[19] Here, the UPS spectra of the $MAPbI_3$ films with precursor ratio of 1.0, 0.65, and 0.3 was collected once again for the completeness. As shown in Supporting Information Figure S1, it is found that the work function (WF) increases while the VBM shifts toward the Fermi energy (E_F) as the precursor ratio decreases from 1.0 to 0.3, indicating the WF and VBM are clearly influenced by the precursor ratio. The VBM of the $MAPbI_3$ film fabricated from precursor ratio of 1.0 is measured to be 0.9 eV below the E_F, which indicates an n-doped film given the fact that the gap of $MAPbI_3$ is 1.5 eV. The VBM is pushed up to 0.7 eV below the E_F when reducing the precursor ratio to 0.3. A total shift toward to E_F of 0.2 eV for the core levels as well as the VBM indicates a conversion from n-doped film to weakly p-doped film as reducing the precursor ratio from 1.0 to 0.3.

As shown in Figure 2a, the C 1s core level includes two peaks for all $MAPbI_3$ films. The C 1s peaks centered on ca. 284.5 and 285.9 eV are assigned to amorphous carbon and methyl carbons in $MAPbI_3$, respectively.[25−28] Given the $MAPbI_3$ film thickness of 250 nm and no information on sulfur component in the PEDOT:PSS substrate being detected by the XPS spectra of $MAPbI_3$ film, we speculate that the C 1s peak centered on ca. 284.5 eV does not originate from the carbon component of the PEDOT:PSS substrate. The amorphous carbon component is stronger than the other one, which should be ascribed to the carbon contamination coming from the environment during the preparation and the subsequent annealing process. Both the N 1s and I $3d_{5/2}$ core level include a single peak as shown in Figure 2b and c, indicating the only one N and I component in the $MAPbI_3$ films.[26,29] From Figure 2d, we can find that the Pb $4f_{7/2}$ core level comprises of two components represented by two peaks centered on ca. 137.9 and 136.3 eV, respectively. The bigger one can be associated with the Pb component in $MAPbI_3$ structure, while the much smaller one to metallic Pb decomposed from PbI_2 due to the chemical reaction during the sample annealing process as $MAPbI_3$ films were prepared.[30−32] The conclusion obtained here agrees well with that reported by Lindblad et al.[33] in which they observed two similar peaks for the Pb $4f_{7/2}$ core level with the energy difference of 1.7 eV between them.

To investigate the annealing effect on the electronic properties of the film at different temperature, the $MAPbI_3$ film fabricated with 0.3 precursor ratio was chosen to carry out annealing treatment. As shown in Figure 3a,b, the XPS spectra of I 3d and Pb 4f are collected for the annealed $MAPbI_3$ film at 110 °C for 30 min and 150 °C for 45 min. By comparison, the XPS spectra of I 3d and Pb 4f is also presented for the as-grown $MAPbI_3$ film with 0.3 precursor ratio. Because of spin−orbital splitting, I 3d core level is a doublet consisting of the I $3d_{5/2}$ and I $3d_{3/2}$ components separated by 11.5 eV and with a branching ratio of 1.5.[31] For the Pb 4f core level, it is a doublet consisting of Pb $4f_{7/2}$ and Pb $4f_{5/2}$ components with an energy separation of 4.85 eV.[31,33] Naturally, the small peaks in the Pb 4f spectra at the lower binding energy compared with the main peak are associated with metallic lead. It is observed that the binding energies of I 3d and Pb 4f core level remain unchanged after annealing at 110 °C (see the dashed lines), supporting the results observed by the UPS spectra of $MAPbI_3$ films as shown in Supporting Information Figure S1. The intensity of XPS spectra increase significantly likely due to the removal of surface

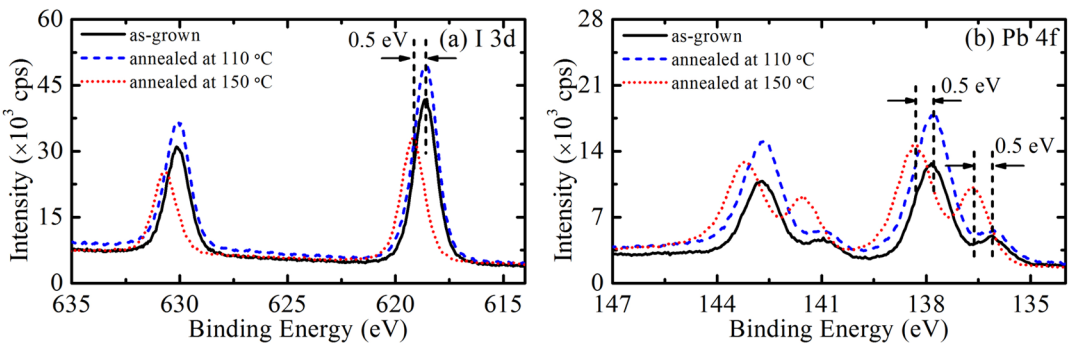

Figure 3. XPS spectra of (a) I 3d and (b) Pb 4f for the $MAPbI_3$ film fabricated with 0.3 precursor ratio. The solid, dashed, and dotted lines denote the spectra of the as-grown $MAPbI_3$, the corresponding annealed film at 110 °C for 30 min and that at 150 °C for 45 min, respectively.

DOI: 10.1021/acs.jpcc.5b07728
J. Phys. Chem. C 2016, 120, 215−220

contaminations and/or the modification of the film morphology during the annealing process. It is confirmed that an annealing at such a low temperature of 110 °C could not change the electronic properties of the $MAPbI_3$ film. However, the core levels of I 3d and Pb 4f obviously shift back to higher BE by ca. 0.5 eV for the $MAPbI_3$ film annealed at 150 °C (see the dotted lines) compared with the as-grown $MAPbI_3$ film, which is qualitatively consistent with the VBM shift observed in UPS. As shown in Supporting Information Figure S1, the VBM of the annealed $MAPbI_3$ film at 150 °C is pushed down to 1.3 eV from 0.7 eV below the E_F, indicating a down shift of 0.6 eV. We can conclude that the weakly p-doped $MAPbI_3$ film can be converted into strong n-doped film through this annealing treatment at such a temperature of up to 150 °C. Therefore, the results observed here indicate that the electronic structure of $MAPbI_3$ film can be changed by implementing an appropriate annealing process. Interestingly, the shift of both C 1s and N 1s core levels show an unexpected behavior with the slight shifts to lower BE after annealing (not showing here), which may be perhaps associated with the complex chemical reactions occurred during the annealing process, although further research is needed to understand the exact reasons. The chemical reaction to some extent is further confirmed by the existence of the strong metallic Pb component. The metallic Pb-related peak is observed to rise obviously after the annealing at 150 °C, indicating that more metallic Pb is decomposed from PbI_2 or segregated from $MAPbI_3$ during the annealing process.

Table 1 presents the elemental composition in $MAPbI_3$ films with different precursor ratios. The amorphous C and the metallic Pb are separated from the basic components as impurity ones. The elemental compositions of the C and N increase as the precursor ratios decrease, which can be attributed to the increase of the MAI content in the precursor solution, while the elemental composition of the Pb decrease with decreasing the PbI_2 content. Since PbI_2 has a better affinity to the PEDOT:PSS substrate than MAI, a net drop of the I content was observed with the decrease of PbI_2 despite the increase of MAI in the precursor solution.[19] Yin's calculation results argued that Pb default would form p-type film and I default form n-type film in perovskite materials.[34] Therefore, the deficiency of PbI_2 in precursor mixture solution will lead to the formation of Pb vacancies and thus achieving a p-type film as observed previously in the UPS results. For the $MAPbI_3$ film fabricated with 0.3 precursor ratio after a 150 °C annealing for 45 min, it is found that the elemental compositions of the I and N decrease sharply while the Pb increases slightly, thus, I vacancies would be formed by the reduction of the I content and an n-type film is naturally achieved according to Yin's report. The reductions of the I and N can be ascribed to the evaporation of MAI from the $MAPbI_3$ films during the annealing process. As reported by our recent investigation,[35] the other possible reason about the I reduction is associated with the formation of volatile I by passing the electron of I^- to Pb^{2+} and becoming neutral, which in turn escapes to the vacuum. Meanwhile, more metallic Pb was detected compared with the situation before 150 °C annealing as confirmed by the bigger peak of metallic Pb in Figure 3b. Furthermore, it is worth noting that there are obvious deviations from stoichiometric $MAPbI_3$ film, too much C component in particular, which should be partly ascribed to the special distribution of different components in the bulk and surface regions of the $MAPbI_3$ films.

To further analyze the distribution of all components in the bulk and surface regions of the $MAPbI_3$ films, AR-XPS is used for the $MAPbI_3$ film fabricated with 0.3 precursor ratio. As shown in Figure 4, the atomic concentrations of all components including impurity amorphous C and metallic Pb are plotted as a function of the takeoff angle θ for the as-grown film and the corresponding annealed film at 150 °C. The measurement geometry of AR-XPS is shown in the inset of Figure 4a. The probing depth, that is, $\lambda \cos \theta$, where λ is the mean diffusion length of electron in $MAPbI_3$ film, decreases with the increase of takeoff angle, indicating that the larger takeoff angle can be used to reflect the content composition of film closer to the surface.[36,37]

As shown in Figure 4a, the methyl carbon component of the as-grown film decreases as the takeoff angle increases from 0 to 60°, which indicates that more methyl C is distributed in the bulk than in the surface of $MAPbI_3$ film, while the amorphous C shows an inverse distribution. Too much C detected in XPS measurement is possibly associated with the surface preference of the amorphous C originated from the environmental contaminants and the migration of decomposed C toward surface from the bulk region. The I fraction decreases slightly as the takeoff angle increases, indicating that there is more I in the bulk than in the surface region of the $MAPbI_3$ film. The amounts of N and Pb remain nearly unchanged as the takeoff

Table 1. Elemental Composition in $MAPbI_3$ Films with Different Precursor Ratios

PbI_2/MAI	1.0	0.65	0.3	0.3 annealed[a]
C	10.26%	21.03%	25.47%	21.06%
N	5.20%	6.23%	7.14%	1.61%
I	39.61%	25.16%	13.44%	7.93%
Pb	18.34%	10.10%	5.38%	5.41%
amorphous C	25.19%	36.90%	47.25%	60.74%
metallic Pb	1.39%	0.59%	1.32%	3.25%

[a]Denote the $MAPbI_3$ film with the precursor ratio of 0.3 after a 150 °C annealing for 45 min.

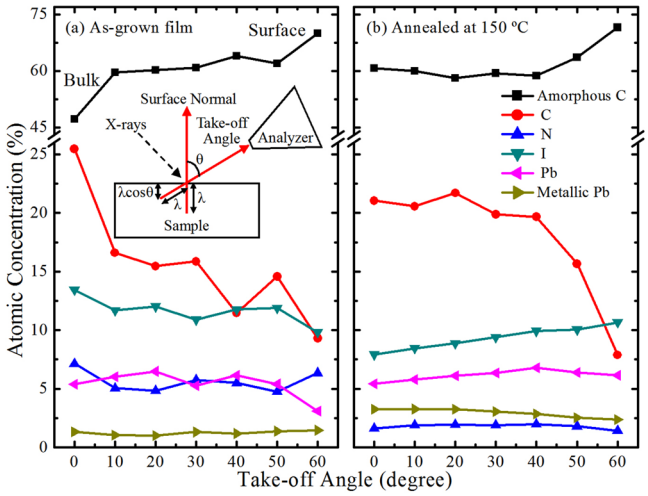

Figure 4. Atomic concentration of all components in the $MAPbI_3$ film with 0.3 precursor ratio as a function of the takeoff angle for (a) the as-grown film and (b) the corresponding film annealed at 150 °C. The inset is the measurement geometry of AR-XPS.

DOI: 10.1021/acs.jpcc.5b07728
J. Phys. Chem. C 2016, 120, 215−220

angle increases, showing a homogeneous distribution in the $MAPbI_3$ film.

It is worth noting that the atomic concentrations of the four compositions are influenced by the annealing process. As shown in Figure 4b, the I and N fraction in the $MAPbI_3$ film present obvious reductions as a whole for all takeoff angles compared with those in Figure 4a, while the Pb fraction increases as illustrated partly in Table 1. The fraction of I and Pb (not including the metallic Pb) increase approximately with increasing takeoff angle, indicating that the higher I and Pb concentration in the surface region than in the bulk is most likely due to the existence of PbI_2 on the surface, which is from decomposition of $MAPbI_3$ by annealing at 150 °C.[38]

To highlight the distribution of all components shown in Figure 5, we plot the relative depths of all chemical components

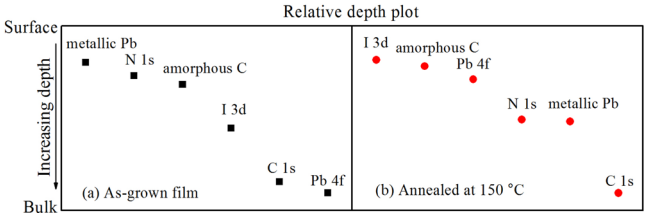

Figure 5. Relative depth plot of chemical components for (a) as-grown film with 0.3 precursor ratio and (b) the corresponding film annealed at 150 °C.

in the $MAPbI_3$ film with 0.3 precursor ratio before and after annealing at 150 °C by using the AR-XPS data. This plot uses the relative sensitivity of each chemical component with respect to the takeoff angle, which allows sorting the components as a function of depth. The relative depth is calculated from the ratio of relative intensities, $\ln(I_{\text{surface angle}}/I_{\text{bulk angle}})$ for each component, where $I_{\text{surface angle}}$ represents the intensity at takeoff angle of 60°, and $I_{\text{bulk angle}}$ represents the intensity at takeoff angle of 0°.[39] It is observed that the metallic Pb, amorphous C and N have smaller relative depth, the C and Pb components have greater relative depth, and the I component has a moderate relative depth for the as-grown $MAPbI_3$ film as shown in Figure 5a. However, the relative depths of the I and Pb components have reduced greatly due to the annealing treatment as shown in Figure 5b, which can be associated with the decomposition of $MAPbI_3$, thus more PbI_2 distribution at the surface region after annealing, as discussed in the previous subsection. In contrast, the relative depths of the N and metallic Pb have increased obviously accompanying the annealing process. We speculate that the relatively small concentration of N in the surface region may be ascribed to the evaporation of MAI and the deeper relative position of the metallic Pb indicates its infiltration into the bulk via the annealing treatment. The relative depth of the amorphous C remains almost unchanged, which supports its surface preference.

4. CONCLUSIONS

We have investigated the electronic structure and surface composition of the $MAPbI_3$ films fabricated by one-step method with different precursor ratios using UPS and XPS. The results observed here show that the electronic properties and the surface composition of the $MAPbI_3$ film are dependent on the precursor ratio and annealing process. The $MAPbI_3$ films with different electronic properties can be prepared by regulate precursor ratio or annealing. Furthermore, AR-XPS results show that the relative depths of all components are influenced by annealing treatment and an annealing at 150 °C leads to the relatively shallow distribution of I and Pb components in the $MAPbI_3$ film and the infiltration of metallic Pb into the bulk. Our analysis here provides insight for the underlining mechanisms in controlling the electrical properties of $MAPbI_3$ films by precursor ratios and annealing, which in turn will be useful for fabricating high efficiency $MAPbI_3$ solar cells.

■ ASSOCIATED CONTENT

Supporting Information

The Supporting Information is available free of charge on the ACS Publications website at DOI: 10.1021/acs.jpcc.5b07728.

The UPS spectra of $MAPbI_3$ films with different precursor ratios and complete refs 35 and 37. (PDF)

■ AUTHOR INFORMATION

Corresponding Authors

*E-mail: (X.L.) xl_liu@csu.edu.cn. Tel.: +86-731-88830323.
*E-mail: (Y.G.) ygao@pas.rochester.edu. Tel.: +86-731-88830323.

Notes

The authors declare no competing financial interest.

■ ACKNOWLEDGMENTS

We thank the financial support by the National Natural Science Foundation of China (Grants 51173205, 11334014). Y.G. thanks the National Science Foundation (Grant CBET-1437656). H.X. acknowledges the Innovation Fund for Graduate Students of CSU (2014ZZTS011). X.L. acknowledges the National Training Programs of Innovation and Entrepreneurship for Undergraduates of China (1401130141). J.H. thanks the National Science Foundation under Awards DMR-1505535 and ECCS-1252623.

■ REFERENCES

(1) Jeng, J. Y.; Chiang, Y. F.; Lee, M. H.; Peng, S. R.; Guo, T. F.; Chen, P.; Wen, T. C. $CH_3NH_3PbI_3$ Perovskite/Fullerene Planar-Heterojunction Hybrid Solar Cells. *Adv. Mater.* **2013**, *25*, 3727−3732.
(2) Abrusci, A.; Stranks, S. D.; Docampo, P.; Yip, H. L.; Jen, A. K. Y.; Snaith, H. J. High-performance Perovskite-Polymer Hybrid Solar Cells via Electronic Coupling with Fullerene Monolayers. *Nano Lett.* **2013**, *13*, 3124−3128.
(3) Zhao, Y. X.; Zhu, K. Charge Transport and Recombination in Perovskite $CH_3NH_3PbI_3$ Sensitized TiO_2 Solar Cells. *J. Phys. Chem. Lett.* **2013**, *4*, 2880−2884.
(4) Chen, Q.; Zhou, H. P.; Hong, Z. R.; Luo, S.; Duan, H. S.; Wang, H. H.; Liu, Y. S.; Li, G.; Yang, Y. Planar Heterojunction Perovskite Solar Cells via Vapor-Assisted Solution Process. *J. Am. Chem. Soc.* **2014**, *136*, 622−625.
(5) Kojima, A.; Teshima, K.; Shirai, Y.; Miyasaka, T. Organometal Halide Perovskites as Visible-Light Sensitizers for Photovoltaic Cells. *J. Am. Chem. Soc.* **2009**, *131*, 6050−6051.
(6) Ball, J. M.; Lee, M. M.; Hey, A.; Snaith, H. J. Low-Temperature Processed Meso-superstructured to Thin-Film Perovskite Solar Cells. *Energy Environ. Sci.* **2013**, *6*, 1739−1743.
(7) Burschka, J.; Pellet, N.; Moon, S. J.; Humphry-Baker, R.; Gao, P.; Nazeeruddin, M. K.; Grätzel, M. Sequential Deposition as a Route to High-Performance Perovskite-Sensitized Solar Cells. *Nature* **2013**, *499*, 316−320.
(8) Bi, C.; Wang, Q.; Shao, Y. C.; Yuan, Y. B.; Xiao, Z. G.; Huang, J. S. Non-Wetting Surface-Driven High-Aspect-Ratio Crystalline Grain

Growth for Efficient Hybrid Perovskite Solar Cells. *Nat. Commun.* **2015**, *6*, 7747.
(9) Yang, W. S.; Noh, J. H.; Jeon, N. J.; Kim, Y. C.; Ryu, S.; Seo, J.; Seok, S. High-Performance Photovoltaic Perovskite Layers Fabricated Through Intramolecular Exchange. *Science* **2015**, *348*, 1234−1237.
(10) Lee, M. M.; Teuscher, J.; Miyasaka, T.; Murakami, T. N.; Snaith, H. J. Efficient Hybrid Solar Cells Based on Meso-Superstructured Organometal Halide Perovskites. *Science* **2012**, *338*, 643−647.
(11) Xiao, Z. G.; Bi, C.; Shao, Y. C.; Dong, Q. F.; Wang, Q.; Yuan, Y. B.; Wang, C. G.; Gao, Y. L.; Huang, J. S. Efficient, High Yield Perovskite Photovoltaic Devices Grown by Interdiffusion of Solution-Processed Precursor Stacking Layers. *Energy Environ. Sci.* **2014**, *7*, 2619−2623.
(12) Kim, H. B.; Choi, H.; Jeong, J.; Kim, S.; Walker, B.; Song, S.; Kim, J. Y. Mixed Solvents for the Optimization of Morphology in Solution-Processed, Inverted-Type Perovskite/Fullerene Hybrid Solar Cells. *Nanoscale* **2014**, *6*, 6679−6683.
(13) Malinkiewicz, O.; Yella, A.; Lee, Y. H.; Espallargas, G. M.; Graetzel, M.; Nazeeruddin, M. K.; Bolink, H. J. Perovskite Solar Cells Employing Organic Charge-Transport Layers. *Nat. Photonics* **2013**, *8*, 128−132.
(14) Liu, M. Z.; Johnston, M. B.; Snaith, H. J. Efficient Planar Heterojunction Perovskite Solar Cells by Vapour Deposition. *Nature* **2013**, *501*, 395−398.
(15) Zhao, Y. X.; Zhu, K. Solution Chemistry Engineering toward High-Efficiency Perovskite Solar Cells. *J. Phys. Chem. Lett.* **2014**, *5*, 4175−4186.
(16) Jeon, N. J.; Noh, J. H.; Kim, Y. C.; Yang, W. S.; Ryu, S.; Seok, S. Solvent Engineering for High-Performance Inorganic-Organic Hybrid Perovskite Solar cells. *Nat. Mater.* **2014**, *13*, 897−903.
(17) Lim, K. G.; Kim, H. B.; Jeong, J.; Kim, H.; Kim, J. Y.; Lee, T. W. Boosting the Power Conversion Efficiency of Perovskite Solar Cells Using Self-Organized Polymeric Hole Extraction Layers with High Work Function. *Adv. Mater.* **2014**, *26*, 6461−6466.
(18) Kim, Y. H.; Cho, H.; Heo, J. H.; Kim, T. S.; Myoung, N.; Lee, C. L.; Im, S. H.; Lee, T. W. Multicolored Organic/Inorganic Hybrid Perovskite Light-Emitting Diodes. *Adv. Mater.* **2015**, *27*, 1248−1254.
(19) Wang, Q.; Shao, Y. C.; Xie, H. P.; Lyu, L.; Liu, X. L.; Gao, Y. L.; Huang, J. S. Qualifying Composition Dependent *p* and *n* Self-Doping in $CH_3NH_3PbI_3$. *Appl. Phys. Lett.* **2014**, *105*, 163508.
(20) Wang, Q.; Shao, Y. C.; Dong, Q. F.; Xiao, Z. G.; Yuan, Y. B.; Huang, J. S. Large Fill-Factor Bilayer Iodine Perovskite Solar Cells Fabricated by a Low-Temperature Solution-Process. *Energy Environ. Sci.* **2014**, *7*, 2359−2365.
(21) Zhang, L.; Yang, Y. G.; Huang, H.; Lyu, L.; Zhang, H.; Cao, N. T.; Xie, H. P.; Gao, X. Y.; Niu, D. M.; Gao, Y. L. Thickness-Dependent Air-Exposure-Induced Phase Transition of CuPc Ultrathin Films to Well-Ordered One-Dimensional Nanocrystals on Layered Substrates. *J. Phys. Chem. C* **2015**, *119*, 4217−4223.
(22) Xie, H. P.; Huang, H.; Cao, N. T.; Zhou, C. H.; Niu, D. M.; Gao, Y. L. Effects of Annealing on Structure and Composition of LSMO Thin Films. *Phys. B* **2015**, *477*, 14−19.
(23) Liu, X. L.; Yi, S. J.; Wang, C. G.; Wang, C. C.; Irfan, I.; Gao, Y. L. Electronic Structure Evolution and Energy Level Alignment at C_{60}/TAPC/MoO_x/ITO interfaces. *J. Appl. Phys.* **2014**, *115*, 163708.
(24) Liu, X. L.; Wang, C. G.; Wang, C. C.; Irfan, I.; Gao, Y. L. Interfacial Electronic Structures of Buffer-modified C_{60}/Pentacene-Based Charge Generation Layer. *Org. Electron.* **2015**, *17*, 325−333.
(25) Kim, Y. J.; Park, C. R. Analysis of Problematic Complexing Behavior of Ferric Chloride with N,N-Dimethylformamide using Combined Techniques of FT-IR, XPS, and TGA/DTG. *Inorg. Chem.* **2002**, *41*, 6211−6216.
(26) Chen, S.; Goh, T. W.; Sabba, D.; Chua, J.; Mathews, N.; Huan, C. H. A.; Sum, T. C. Energy Level Alignment at the Methylammonium Lead Iodide/Copper Phthalocyanine Interface. *APL Mater.* **2014**, *2*, 081512.
(27) Liu, X. L.; Wang, C. G.; Lyu, L.; Wang, C. C.; Xiao, Z. G.; Bi, C.; Huang, J. S.; Gao, Y. L. Electronic Structures at the Interface between Au and $CH_3NH_3PbI_3$. *Phys. Chem. Chem. Phys.* **2015**, *17*, 896−902.
(28) Wang, C. G.; Wang, C. C.; Liu, X. L.; Kauppi, J.; Shao, Y. C.; Xiao, Z. G.; Bi, C.; Huang, J. S.; Gao, Y. L. Electronic Structure Evolution of Fullerene on $CH_3NH_3PbI_3$. *Appl. Phys. Lett.* **2015**, *106*, 111603.
(29) Zheng, Z.; Liu, A. R.; Wang, S. M.; Wang, Y.; Li, Z. S.; Lau, W. M.; Zhang, L. Z. In Situ Growth of Epitaxial Lead Iodide Films Composed of Hexagonal Single Crystals. *J. Mater. Chem.* **2005**, *15*, 4555−4559.
(30) Liu, S. L.; Zhang, L.; Li, Y. R.; Han, M.; Dai, Z. H.; Bao, J. C. Synthesis of PbS/PbI_2 Nanocomposites in Mixed Solvent and their Composition-Dependent Electrogenerated Chemiluminescence Performance. *Inorg. Chem.* **2014**, *53*, 8548−8554.
(31) Chastain, J.; Moulder, J. F. *Handbook of X-ray Photoelectron Spectroscopy: A Reference Book of Standard Spectra for Identification and Interpretation of XPS Data*; Physical Electronics Division; Perkin-Elmer Corporation: Eden Prairie, MN, 1995.
(32) Raga, S. R.; Jung, M. C.; Lee, M. V.; Leyden, M. R.; Kato, Y.; Qi, Y. B. Influence of Air Annealing on High Efficiency Planar Structure Perovskite Solar Cells. *Chem. Mater.* **2015**, *27*, 1597−1603.
(33) Lindblad, R.; Bi, D. Q.; Park, B.; Oscarsson, J.; Gprgoi, M.; Siegbahn, H.; Odelius, M.; Johansson, E. M. J.; Rensmo, H. Electronic Structure of TiO_2-$CH_3NH_3PbI_3$ Perovskite Solar Cell Interfaces. *J. Phys. Chem. Lett.* **2014**, *5*, 648−653.
(34) Yin, W. J.; Shi, T. T.; Yan, Y. F. Unusual Defect Physics in $CH_3NH_3PbI_3$ Perovskite Solar Cell Absorber. *Appl. Phys. Lett.* **2014**, *104*, 063903.
(35) Liu, P.; Liu, X. L.; Lyu, L.; Xie, H. P.; Zhang, H.; Niu, D. M.; Huang, H.; Bi, C.; Xiao, Z. G.; Huang, J. S.; et al. Interfacial Electronic Structure at the $CH_3NH_3PbI_3$/MoO_x Interface. *Appl. Phys. Lett.* **2015**, *106*, 193903.
(36) Liu, X. L.; Wang, C. G.; Irfan, I.; Yi, S. J.; Gao, Y. L. Effect of Oxygen Plasma Treatment on Air Exposed MoO_x Thin Film. *Org. Electron.* **2014**, *15*, 977−983.
(37) Colella, S.; Mosconi, E.; Pellegrino, G.; Alberti, A.; Guerra, V. L. P.; Masi, S.; Listorti, A.; Rizzo, A.; Condorelli, G. G.; De Angelis, F.; et al. Elusive Presence of Chloride in Mixed Halide Perovskite Solar Cells. *J. Phys. Chem. Lett.* **2014**, *5*, 3532−3538.
(38) Philippe, B.; Park, B. W.; Lindblad, R.; Oscarsson, J.; Ahmadi, S.; Johansson, E. M. J.; Rensmo, H. Chemical and Electronic Structure Characterization of Lead Halide Perovskites and Stability Behavior under Different Exposures-A Photoelectron Spectroscopy Investigation. *Chem. Mater.* **2015**, *27*, 1720−1731.
(39) Kazansky, L. P.; Selyaninov, I. A.; Kuznetsov, Y. I. Angle Resolved XPS of Monomolecular Layer of 5-chlorobenzotriazole on Oxidized Metallic Surface. *Appl. Surf. Sci.* **2012**, *259*, 385−392.

DOI: 10.1021/acs.jpcc.5b07728
J. Phys. Chem. C 2016, 120, 215−220